

MIT Open Access Articles

Rapid and extensive warming following cessation of solar radiation management

The MIT Faculty has made this article openly available. **Please share** how this access benefits you. Your story matters.

Citation: McCusker, Kelly E, Kyle C Armour, Cecilia M Bitz, and David S Battisti. "Rapid and Extensive Warming Following Cessation of Solar Radiation Management." *Environmental Research Letters* 9, no. 2 (January 1, 2014): 024005.

As Published: <http://dx.doi.org/10.1088/1748-9326/9/2/024005>

Publisher: Institute of Physics Publishing

Persistent URL: <http://hdl.handle.net/1721.1/86305>

Version: Final published version: final published article, as it appeared in a journal, conference proceedings, or other formally published context

Terms of use: Creative Commons Attribution



Rapid and extensive warming following cessation of solar radiation management

This content has been downloaded from IOPscience. Please scroll down to see the full text.

2014 Environ. Res. Lett. 9 024005

(<http://iopscience.iop.org/1748-9326/9/2/024005>)

View [the table of contents for this issue](#), or go to the [journal homepage](#) for more

Download details:

IP Address: 18.51.1.88

This content was downloaded on 03/04/2014 at 15:36

Please note that [terms and conditions apply](#).

Rapid and extensive warming following cessation of solar radiation management

Kelly E McCusker¹, Kyle C Armour², Cecilia M Bitz³ and David S Battisti³

¹ School of Earth and Ocean Sciences, University of Victoria, Victoria, BC, Canada

² Department of Earth, Atmospheric and Planetary Sciences, Massachusetts Institute of Technology, Cambridge, MA, USA

³ Department of Atmospheric Sciences, University of Washington, Seattle, WA, USA

E-mail: kemccusk@uvic.ca

Received 14 July 2013, revised 22 January 2014

Accepted for publication 24 January 2014

Published 17 February 2014

Abstract

Solar radiation management (SRM) has been proposed as a means to alleviate the climate impacts of ongoing anthropogenic greenhouse gas (GHG) emissions. However, its efficacy depends on its indefinite maintenance, without interruption from a variety of possible sources, such as technological failure or global cooperation breakdown. Here, we consider the scenario in which SRM—via stratospheric aerosol injection—is terminated abruptly following an implementation period during which anthropogenic GHG emissions have continued. We show that upon cessation of SRM, an abrupt, spatially broad, and sustained warming over land occurs that is well outside 20th century climate variability bounds. Global mean precipitation also increases rapidly following cessation, however spatial patterns are less coherent than temperature, with almost half of land areas experiencing drying trends. We further show that the rate of warming—of critical importance for ecological and human systems—is principally controlled by background GHG levels. Thus, a risk of abrupt and dangerous warming is inherent to the large-scale implementation of SRM, and can be diminished only through concurrent strong reductions in anthropogenic GHG emissions.

Keywords: climate engineering, geoengineering, solar radiation management, abrupt climate change


 Online supplementary data available from stacks.iop.org/ERL/9/024005/mmedia

1. Introduction

Stratospheric aerosol injection has emerged as a popular, hypothetical solar radiation management (SRM) technique due to its technological and economic feasibility and potential to swiftly and effectively cool the planet and avoid impending climate emergencies (Keith *et al* 2010, Vaughan and Lenton 2011). Moreover, the observed cooling following volcanic eruptions (Robock 2000) and numerical simulations of SRM within climate models (e.g. Rasch *et al* 2008a, Robock *et al* 2008, Ammann *et al* 2010, McCusker *et al* 2012) serve as

strong evidence that an enhanced stratospheric aerosol layer could effectively curb global warming. In order to stabilize global climate near present-day conditions, SRM would need to provide a negative shortwave radiative forcing that is comparable to the current global energy imbalance, observed to be on the order of 0.5–1 W m² (Hansen *et al* 2011, Lyman *et al* 2010). Of course, as greenhouse gas (GHG) emissions continue, the magnitude of SRM forcing required to cool or stabilize global climate will correspondingly increase.

If such an enhanced stratospheric aerosol layer were produced, any interruption to its continual maintenance would cause a quick return to natural aerosol levels within 1–2 years (Rasch *et al* 2008b). In turn, global temperature would increase rapidly as the climate adjusts to the full, unmasked GHG radiative forcing. Previous evaluations of SRM termination

 Content from this work may be used under the terms of the [Creative Commons Attribution 3.0 licence](http://creativecommons.org/licenses/by/3.0/). Any further distribution of this work must maintain attribution to the author(s) and the title of the work, journal citation and DOI.

(Wigley 2006, Matthews *et al* 2007, Ross and Matthews 2009, Brovkin *et al* 2009, Robock *et al* 2008, McCusker *et al* 2012, Irvine *et al* 2012) have focused on the global and annual mean climate response under ‘business-as-usual’ GHG emissions scenarios. These studies suggest that the rates of global warming following SRM cessation could reach 1 °C/decade or greater, far exceeding warming rates had no SRM been implemented. Such a rapid temperature change would substantially affect human and ecological systems, whose resilience would be limited by rates as small as a few tenths of a degree per decade (van Vliet and Leemans 2006, Lenton 2011).

Of critical importance for ecosystem adaptation and survival is the geographic structure of warming and the rate of seasonal temperature change (Lenton 2011). Crop yields, for example, are highly sensitive to growing season (typically summertime) temperature, and have already declined in response to 20th century warming (Lobell *et al* 2011). Indeed, major threats to food security have historically been overcome in part by regional food surpluses compensating for low yields in other regions (Battisti and Naylor 2009); more spatially broad and rapid warming could preclude the existence of such compensating regions. Moreover, a high rate of environmental change reduces the mean fitness of populations (Bell and Collins 2008), yielding at minimum, a less diverse group of the ‘luckiest’ species (Bell and Collins 2008) resulting in loss of biodiversity. Survival of migratory animals depends on the distance to their optimal climate and the speed at which they can disperse; many mammals are already at risk of losing pace with climate change (Schloss *et al* 2012). Thus, widespread and rapid warming following SRM cessation could issue a one-two punch to human and ecosystem adaptation.

Motivated by the above assessments of impacts of rapid change on ecosystems and human systems, we first consider here the geographic structure of temperature and precipitation change following SRM cessation, with particular focus on the rates of seasonal warming over land, features lost in the global and temporal averaging of earlier studies. We then analyze the response to SRM cessation over a wide variety of plausible scenarios, spanning a range of climate sensitivities, future GHG emissions trajectories, and SRM termination years. The results are considered in the context of the temperature and precipitation trends experienced over the past century, to which ecosystems and human systems have become well adapted in their respective regions.

2. Geographic pattern of land surface temperature trends

To evaluate the spatial climate response to a SRM termination, we use the Community Climate System Model version 4 (CCSM4) (Gent *et al* 2011), a state-of-the-art fully-coupled general circulation model (GCM). We obtained six CCSM4 20th century simulation (Historical; 1900–2005) ensemble members, 300 years of a Preindustrial control simulation, and a CCSM4 RCP8.5 simulation from the National Center for Atmospheric Research. The RCP8.5 simulation is forced with GHG and aerosol emissions into the future, such that the

radiative forcing reaches about 8.5 W m⁻² above preindustrial levels by 2100 (Moss *et al* 2010). The Historical simulations have slightly varied initial conditions and are identically forced with historical GHG and aerosol emissions plus volcanic eruptions.

To simulate a SRM scenario within CCSM4, we impose in the year 2035 a latitudinally distributed, zonally uniform, monthly climatology of stratospheric sulfate aerosol concentration (as in McCusker *et al* (2012)). At this time, global mean surface air temperature (SAT) is about 1 °C higher than the end of the 20th century (1970–1999 mean) and about 2 °C higher than preindustrial SAT. We increase the prescribed sulfate burden from zero to 8 teragrams of sulfur equivalent (TgS) in 3 years to approximately return to the end of the 20th century temperature, then increase the concentration to provide a roughly equal and opposite radiative forcing to RCP8.5 (at a rate of 0.67 TgS/year) thus approximately stabilizing global climate. To simulate an abrupt SRM cessation, the sulfate burden is zeroed after 25 years of implementation (year 2060). We conduct an ensemble of two such ‘SRM shutoff’ simulations with slightly varied initial conditions.

Following SRM termination, the global average annual mean SAT rapidly approaches the temperature had no SRM been implemented (figure 1). Global mean SAT increases by nearly 4 °C within 30 years, compared to a SAT increase of less than 2 °C in that same time period under the RCP8.5 scenario. The linear trend of global SAT from the 2-member ensemble is 1.16 °C/decade over the first 20 years of the Shutoff scenario, consistent with previous findings (e.g. McCusker *et al* 2012, Irvine *et al* 2012). This trend is about six times larger than the observed global warming trend since 1975 (0.2 °C/decade) (Hansen *et al* 2006) and sixteen times greater than the observed trend over the entire 20th century (0.07 °C/decade) (Hansen *et al* 2006).

We focus here on the spatial pattern of summertime temperature change in each hemisphere (JJA to the north of the equator, and DJF to the south) because of the implications for agricultural productivity, but warming rates for the winter mean and annual mean are consistent with those in summer (see figure S1 available at stacks.iop.org/ERL/9/024005/mmedia). The ensemble land-averaged 5-year summer SAT trend following SRM termination is 3.3 °C/decade, while local trends are as high as 15 °C/decade (figure 2(a)); over much of the northern high latitudes, temperature trends are near 8 °C/decade. The 20-year trends are more spatially homogeneous, with an average trend of 1.25 °C/decade, and many regions near 2–2.5 °C/decade (figure 2(d)).

To put the SRM Shutoff trends into context, we normalize the 5- and 20-year trends by the typical variation (standard deviation) of local simulated historical trends of the same time interval (figures 2(b) and (e)). The historical standard deviation is calculated from distributions of 5- and 20-year trends sampled from the Historical CCSM4 ensemble (further described in supplementary materials available at stacks.iop.org/ERL/9/024005/mmedia). While the 5-year warming trend is on average 1.3 standard deviations of 20th century variability over land, there is substantial spatial variation (figure 2(b)); in many food insecure regions, such as Sub-Saharan Africa

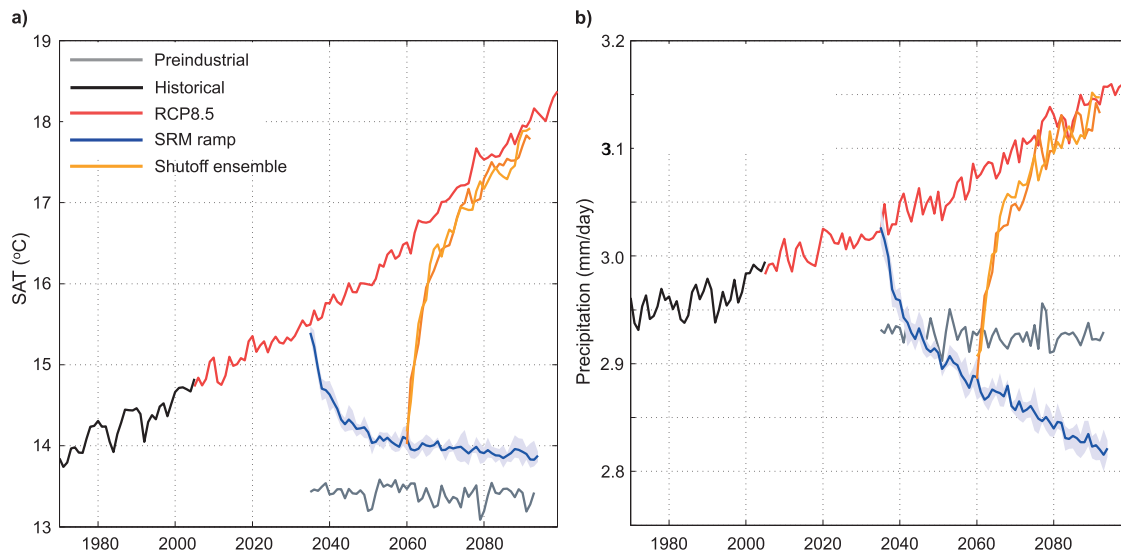


Figure 1. Annual mean, global mean (a) surface air temperature ($^{\circ}\text{C}$) and (b) precipitation (mm/day) for Historical (black), RCP8.5 (red), average of 4 SRM Ramp simulations (blue line) and ensemble range (light blue shading), two SRM Shutoff simulations (orange), and a Preindustrial control (gray) simulation for reference.

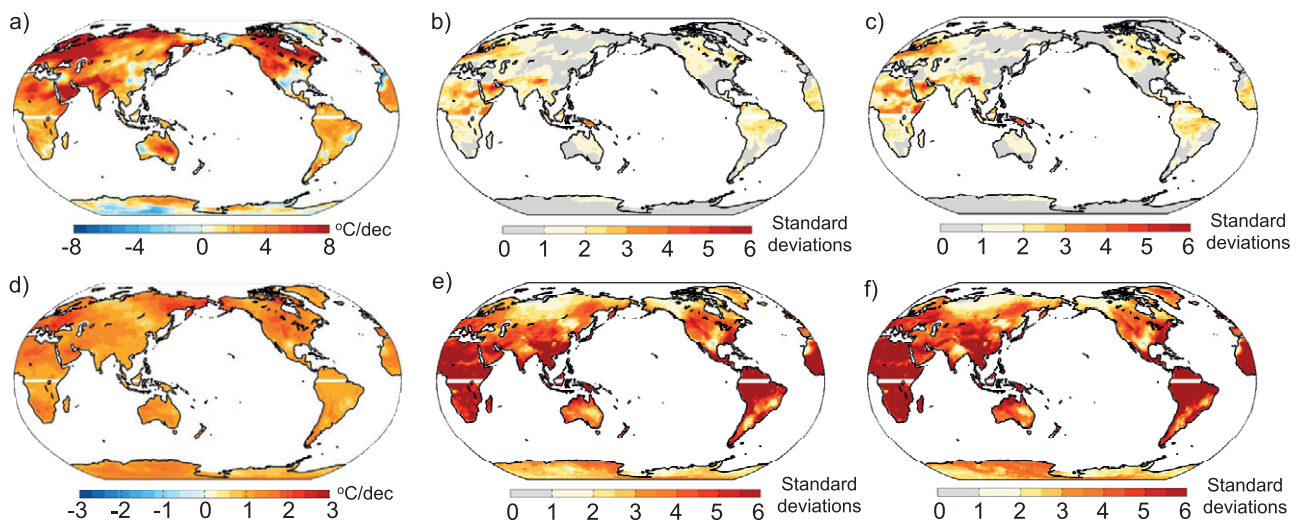


Figure 2. (a) The ensemble average summer 5-year SAT trends ($^{\circ}\text{C}/\text{decade}$) for the period following SRM termination in the Shutoff scenario. (b) The 5-year trends shown in (a), but normalized by the standard deviation of Historical 5-year trends at each grid point. (c) The 5-year trends shown in (a), but normalized by the standard deviation of Preindustrial 5-year trends at each grid point. ((d)–(f)) are as ((a)–(c)), but for 20-year trends. The white stripe at the equator indicates the discontinuity in season from northern hemisphere to southern hemisphere (JJA and DJF, respectively). Trends over the ocean are shown in figure S2 (available at stacks.iop.org/ERL/9/024005/mmedia).

and South Asia (FAO *et al* 2012), trends exceed 2 standard deviations. However, the land-average 20-year warming trend is 4.5 standard deviations of 20th century variability, and local trends exceed two standard deviations in the majority of regions (figure 2(e)). Twenty-year trends are drastically outside of 20th century bounds within the tropics, where variability is relatively small (figure S3 available at stacks.iop.org/ERL/9/024005/mmedia), and exceed 6 standard deviations within many food insecure regions. Annual mean, land-averaged trends are 1.8 and 5.6 standard deviations for 5- and 20-year trends respectively (table 1), and global averages are further out of bounds due to relatively low variability over the world’s oceans

(see figure S2 available at stacks.iop.org/ERL/9/024005/mmedia for global summer trend maps).

The Historical simulations were chosen as the comparison period in order to put trends after SRM cessation into the context of ‘what humans and ecosystems have experienced’ over the previous century, and therefore no detrending was applied to the Historical simulations. Trends normalized by Preindustrial control variability, where no time-varying forcing is included, are generally similar but slightly more anomalous than when normalized by Historical variability, especially over 20 years (table 1, figures 2(c) and (f), and see figures S1 and S2 available at stacks.iop.org/ERL/9/024005/mmedia). We include normalization by both Historical and Preindustrial

Table 1. Shutoff SAT trends. Shutoff summer, winter, and annual average 5- and 20-year SAT trends ($^{\circ}\text{C}/\text{decade}$; leftmost two columns), and normalized trends (rightmost two columns) in which the units are standard deviations (SD) of the respective trend distribution from the Historical simulations, ‘Hist’, and from the Preindustrial simulation, ‘Prei’ in parentheses.

	5yr	20yr	5yr Hist (Prei) SD	20yr Hist (Prei) SD
Summer land	3.3	1.3	1.3 (1.4)	4.5 (5.1)
ocean	2.1	0.9	1.4 (1.5)	5.5 (5.7)
global	2.4	1.0	1.4 (1.5)	4.9 (5.5)
Winter land	4.2	1.4	1.0 (1.0)	3.2 (3.5)
ocean	2.9	1.1	1.4 (1.4)	4.6 (5.1)
global	3.2	1.2	1.3 (1.3)	4.2 (4.6)
ANN land	3.6	1.4	1.8 (1.9)	5.6 (6.8)
ocean	2.7	1.1	2.0 (2.1)	6.4 (7.3)
global	3.0	1.2	1.9 (2.1)	6.2 (7.2)

standard deviation for reference, but focus our analysis mostly on the Historical normalization.

Not only are the trends following SRM cessation large compared to 20th century or preindustrial climate variability, their spatial extensiveness is also unmatched historically. Historical and Preindustrial land SAT trends exhibit a Gaussian shape centered approximately about $0^{\circ}\text{C}/\text{decade}$, indicating that at any given time, about 50% of regional trends would be warming and 50% cooling, with the trends making up the tails occurring rarely (figure S4(a) available at stacks.iop.org/ERL/9/024005/mmedia). Five-year trends especially can be very large ($>8^{\circ}\text{C}/\text{decade}$; figure S4(a) available at stacks.iop.org/ERL/9/024005/mmedia); approaching the magnitude of regional trends following SRM cessation (figure 2(a)). Note that the distribution of Historical 20-year trends is shifted slightly toward more warming trends compared to the Preindustrial control, due to the influence of increasing GHG concentrations.

To further quantify the spatial extensiveness of land SAT trends following SRM cessation, we calculate the probability density distribution across all (area weighted) land grid cells in each ensemble member, for the summer SAT trends following cessation normalized by both the Historical and Preindustrial standard deviations, and their cumulative density distributions (figure S5(a) available at stacks.iop.org/ERL/9/024005/mmedia). Cessation of SRM greatly increases the probability of ‘extreme’ (i.e., trends greater than 2 standard deviations of preindustrial or historical trends; figure S3 available at stacks.iop.org/ERL/9/024005/mmedia) warming trends over land (figure S5(a) available at stacks.iop.org/ERL/9/024005/mmedia). After SRM termination, the probability of extreme, relative to either 20th century or preindustrial variability, 5-year and 20-year summer trends occurring somewhere over land is about 15% and 75%, respectively. Twenty-year summer land trends exceeding 5 standard deviations of historical variability have a probability of nearly 20% (figure S5(a) available at stacks.iop.org/ERL/9/024005/mmedia), and the largest trends tend to occur in the already stressed, less resilient regions in the tropics (figures 2(e) and (f)).

Also important for food production and the ability of ecosystems to withstand rapid heating is the amount of precipitation falling locally—more precipitation could lead to a greater ability of crops and ecosystems to avoid heat stress due to warming. Global average precipitation, unlike global average SAT, is reduced well below Preindustrial values during the period of sulfate geoengineering prior to termination (figure 1(b)) as predicted by Bala *et al* (2008). Upon SRM cessation, global average precipitation rapidly increases as expected (figure 1(b)), and is consistent with the recent results of Jones *et al* (2013).

One might expect there to be greater precipitation on land following SRM cessation due to the land warming faster than the ocean (table 1), which would induce increased monsoon circulations. We find, however, that average 5-year summer precipitation trends on land are negative ($-0.17\text{ mm day}^{-1}/\text{decade}$ compared with $+0.43\text{ mm day}^{-1}/\text{decade}$ over ocean), indicating general drying that would exacerbate the effects of rapid warming. As with the 5-year land SAT trends, the pattern of 5-year precipitation trends shows great spatial variation (figure 3(a)). In particular, the Southeast Asian monsoon region shows rapidly increasing precipitation, greater than $8\text{ mm day}^{-1}/\text{decade}$, and other regions such as Northeast South America, Saudi Arabia, and India experience large drying up to $-8\text{ mm day}^{-1}/\text{decade}$. Nevertheless, this spatial pattern does not persist over 20-year trends, where instead the Indian monsoon shows strengthening and Brazil receives increasing precipitation (figure 3(d)). These trends, especially 5-year trends, are within 2 standard deviations of Historical and Preindustrial variability nearly everywhere over land (figures 3(b), (e), and figure S5(b) available at stacks.iop.org/ERL/9/024005/mmedia). Global precipitation trends are largest over tropical oceans (figure S6 available at stacks.iop.org/ERL/9/024005/mmedia), but, unlike SAT, the variability in 5- and 20-year trends is also largest over oceans (figure S7 available at stacks.iop.org/ERL/9/024005/mmedia).

Perhaps more important for ecosystems and agriculture is how SAT and precipitation change together in a given location. In fact, 49% of the land grid boxes that experience warming trends over a five-year period also experience a drying trend, and 15% of those grid boxes experience extreme warming compared to Historical variability. Forty-six percent of the land grid boxes experience both 20-year warming trends and 20-year drying trends, with almost all locations that experience drying trends also experiencing extreme warming. Coherent spatial relationships between the temperature and precipitation trends are difficult to pick out, but in general, SAT trends are more anomalous than precipitation trends in a given region, especially over 20 years (with the exception of high latitude land; figure S8 available at stacks.iop.org/ERL/9/024005/mmedia), and few regions have SAT and precipitation trends that are both greater than 2 standard deviations. Thus we find that in some regions, the strong positive 20-year warming trends are accompanied by negative trends in precipitation that could compound problems for food production or ecosystem health. However, precipitation patterns should be interpreted with caution. Robust patterns of precipitation change remain elusive in multi-model comparisons of future climate change

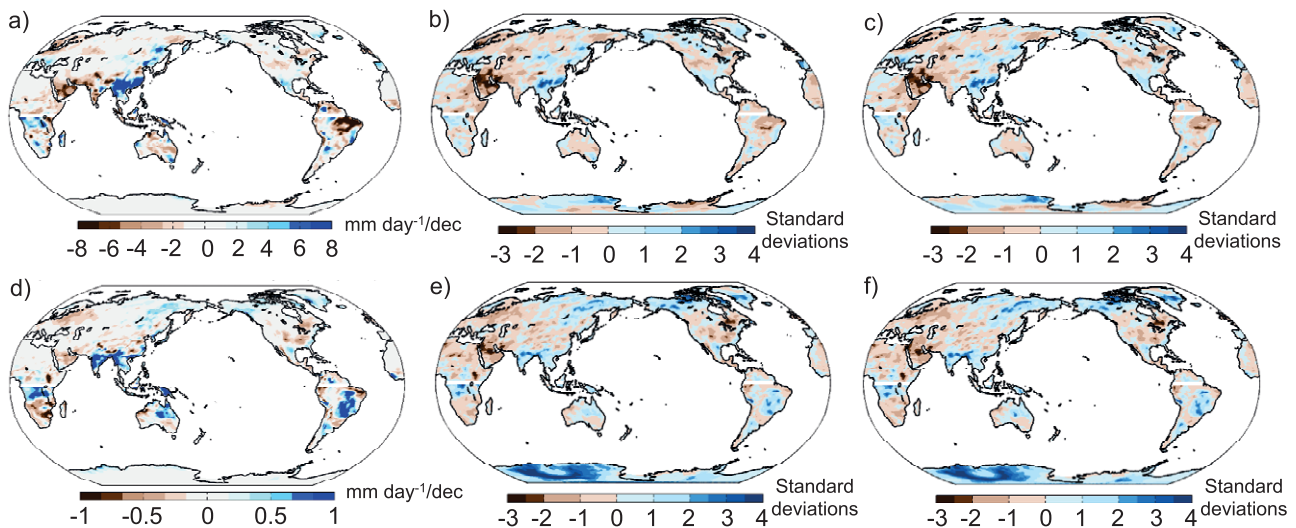


Figure 3. (a) The ensemble average summer 5-year precipitation trends ($\text{mm day}^{-1}/\text{decade}$) for the period following SRM termination in the Shutoff scenario. (b) The 5-year trends shown in (a), but normalized by the standard deviation of Historical 5-year trends at each grid point. (c) The 5-year trends shown in (a), but normalized by the standard deviation of Preindustrial 5-year trends at each grid point. ((d)–(f) are as ((a)–(c)), but for 20-year trends. The white stripe at the equator indicates the discontinuity in season from northern hemisphere to southern hemisphere (JJA and DJF, respectively). Trends over the ocean are shown in figure S6 (available at stacks.iop.org/ERL/9/024005/mmedia).

(Meehl *et al* 2007), solar geoengineering (Kravitz *et al* 2013), and even following termination of SRM (Jones *et al* 2013). Thus, it is not possible to determine with confidence the precise regions where positive temperature trends will be countered by positive precipitation trends, because there are large precipitation trends associated with natural variability, especially in the tropics, as well as model biases.

The above results show that temperature trends following cessation of SRM could far exceed the familiar bounds of 20th century temperature trends, particularly over land within the low latitudes. Twenty-year temperature trends in particular were found to be highly anomalous, with rates of warming exceeding several degrees per decade, over a very broad region covering the low to mid latitude land masses (figures 2(e) and (f)). These results follow from only a few key aspects of climate: the rapid increase in radiative forcing that would occur upon SRM cessation; the rapid adjustment timescales of the ‘fast’ components of the climate system, such as land (Held *et al* 2010); and the relatively small climate variability of the past century, particularly within the tropics. While these general results are robust across a range of SRM cessation scenarios, the details depend, to some extent, on the climate sensitivity of the GCM we have used, the background GHG emissions scenario we have employed, and our assumptions about the timing of the SRM termination. We thus shift our focus to an evaluation of the degree to which the global and annual mean climate response to SRM cessation is sensitive to these assumptions.

3. Sensitivity to termination year, emissions, and climate sensitivity

Current best estimates of climate sensitivity constrain its value to likely be between 2 and 4.5 °C and very likely exceed

1.5 °C (Meehl *et al* 2007). We thus consider here a climate sensitivity range of 1.5–10 °C (see supplementary materials for more details available at stacks.iop.org/ERL/9/024005/mmedia), and further explore a variety of plausible background GHG emissions scenarios and SRM termination years. We employ a simplified, one-dimensional, climate model that has an upwelling-diffusion ocean and energy balance atmosphere with adjustable climate sensitivity (UD-EBM; from Baker and Roe (2009), similar in form to that in Hoffert *et al* (1980)). When tuned to capture the annual and global mean response of CCSM4—including its equilibrium climate sensitivity of 3.2 °C and transient climate response of 1.7 °C (Bitz *et al* 2012)—the UD-EBM successfully reproduces CCSM4’s SAT trends following SRM cessation (black symbols in figure 5).

The background radiative forcing (RF) within the UD-EBM is prescribed to follow RCP8.5 (Riahi *et al* 2007) and RCP2.6 (van Vuuren *et al* 2007) emissions scenarios, representing ‘business-as-usual’ emissions and strong GHG mitigation, respectively. SRM is simulated by maintaining RF at year 2000 levels until the time of abrupt SRM termination, at which point the RF is set to that of the background GHG emissions scenario until year 2100. Each of these simulations is performed for the range of climate sensitivities described above and for a variety of shutoff years.

We first consider the case in which climate sensitivity is set to that of CCSM4 and SRM is employed to mask the business-as-usual emissions scenario (RCP8.5, as was used in the CCSM4 experiments in figures 1 and 2). When SRM is terminated following a 20-year implementation period (year 2020 in figure 4; blue curve), RF abruptly increases by about 1 W m^{-2} , producing a small spike in the rate of temperature change that quickly decays to the rate of the background RCP8.5 scenario. The 20-year temperature trends following SRM cessation are 0.2–0.6 °C/decade for the range of climate

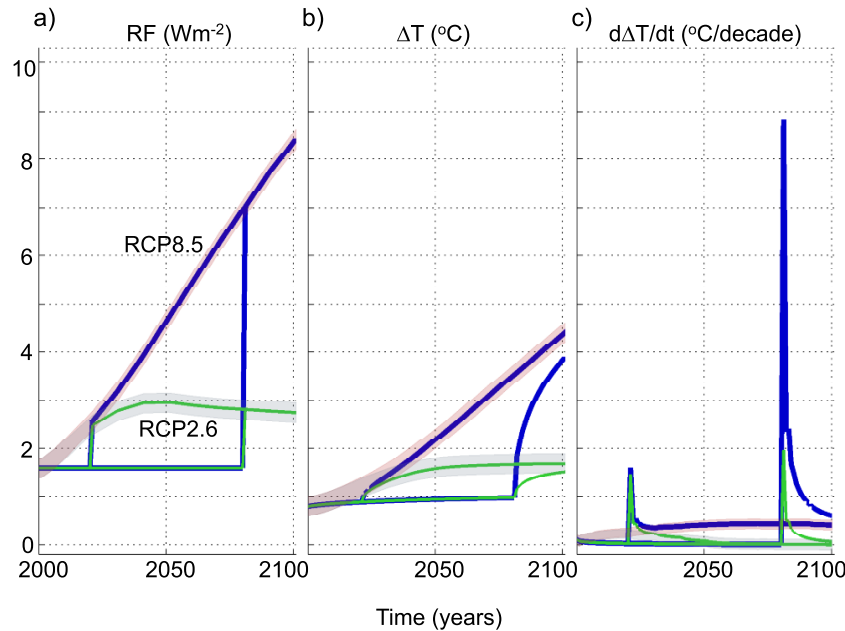


Figure 4. (a) Evolution of the net radiative forcing (RF) due to GHGs and SRM, (b) temperature response (ΔT), and (c) rate of temperature change ($d\Delta T/dt$) with climate sensitivity set to $3.2^{\circ}C$, that of CCSM4. The business-as-usual emissions scenario (RCP8.5) and low-emissions scenario (RCP2.6) are shown in thick, lightly shaded curves (light pink and gray, respectively). SRM termination following 20 years and 80 years of implementation are shown in thinner, dark curves (blue and green for RCP8.5 and RCP2.6 background emissions, respectively). Figure S9 (available at stacks.iop.org/ERL/9/024005/mmedia) displays these results for the ‘very likely’ range of climate sensitivities defined in the Intergovernmental Panel on Climate Change (IPCC) Assessment Report 4 (AR4).

sensitivities (figure 5), comparable to those trends that occur under the RCP8.5 scenario without any SRM.

In contrast, when SRM is implemented for a period of 80 years before cessation, there is an abrupt RF increase of over $5 W m^{-2}$ (year 2080 in figure 4(a); blue curve) due to the loss of the large SRM RF that was required to mask the ongoing accumulation of GHGs in the atmosphere. This spike in RF produces a rapid and substantial increase in global averaged temperature: almost $9^{\circ}C/decade$ in the first few years for CCSM4’s climate sensitivity (figure 4(c)), and up to $10^{\circ}C/decade$ for high climate sensitivities (figure S9 available at stacks.iop.org/ERL/9/024005/mmedia). Sensitivity of initial rates of change are consistent with previous evaluations of SRM termination with multiple climate sensitivities and/or termination year (Matthews *et al* 2007, Ross and Matthews 2009). Twenty-year trends over the range of climate sensitivities are $0.6\text{--}2^{\circ}C/decade$ (figure 5). Thus, under business-as-usual future GHG emissions, the stabilization of climate with SRM for a period of longer than about two decades would create the potential for sustained high rates of warming upon SRM cessation, even if climate sensitivity were near the lower end of its estimated range (figure 5).

We next consider the case where SRM is employed along with concurrent aggressive GHG mitigation measures, as represented by the low-emissions RCP2.6 scenario wherein anthropogenic RF is about $2.6 W m^{-2}$ above preindustrial in 2100 (Moss *et al* 2010). Due to the limited accumulation of GHGs in the atmosphere, the SRM RF required to stabilize climate is relatively small (compared to the RCP8.5 case), and thus SRM termination results in an abrupt RF increase of less than about $2 W m^{-2}$ regardless of its timing (figure 4(a);

green curves). Following SRM cessation, there are high rates of temperature change in the first few years (figure 4(c); green curves), but 20-year temperature trends remain below about $0.4^{\circ}C/decade$ —comparable to those trends that occur under the RCP2.6 scenario without any SRM—over the full range of climate sensitivity and timing of SRM termination (figure 5).

Within each of the above scenarios, the initial rate of temperature change following SRM cessation depends on climate sensitivity only nominally (see supplementary note and figure S10 available at stacks.iop.org/ERL/9/024005/mmedia). Climate sensitivity does become an important factor in setting longer-term temperature trends, particularly under a large RF increase (compare 20-year trends in figure 5 with 5-year trends in figure S10 available at stacks.iop.org/ERL/9/024005/mmedia). However, figure 5 (and figure S10 available at stacks.iop.org/ERL/9/024005/mmedia) shows that the principal control on the rate of temperature change following SRM cessation is the size of the abrupt RF increase, which, in turn, is determined jointly by the background GHG emissions scenario and the duration of time that SRM has been deployed.

Critically then, even for the lowest plausible values of climate sensitivity, decadal temperature trends would be extremely large (double that of the largest 20-year historical trend in CCSM4; horizontal black line in figure 5) in the event of a late 21st century SRM termination under high (RCP8.5) future emissions (figure 5; blue asterisks); conversely, even for the highest plausible values of climate sensitivity, decadal temperature trends would remain relatively small in the event of SRM cessation at any point in the 21st century, under low (RCP2.6) future emissions (figure 5; green asterisks). Thus, the only way to avoid creating the risk of substantial temperature

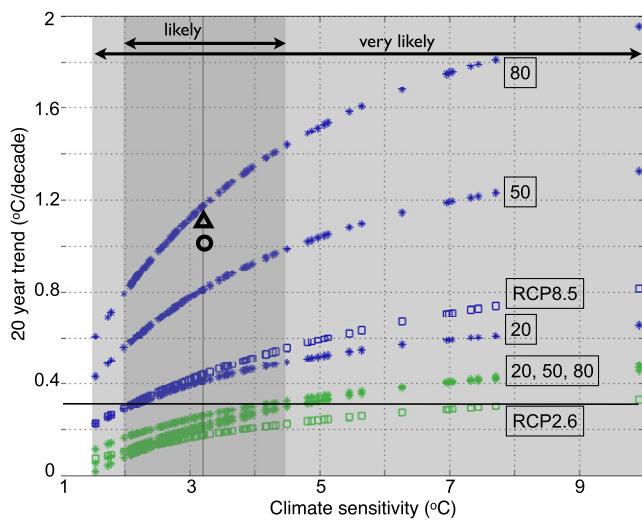


Figure 5. Twenty-year temperature trend following SRM termination — after 20, 50, and 80 years (boxed numbers) of implementation — as a function of climate sensitivity for the RCP8.5 (blue asterisks) and RCP2.6 (green asterisks) background emissions scenarios and the maximum RCP8.5 (blue squares) and RCP2.6 (green squares) 20-year trends. Background shading indicates the Intergovernmental Panel on Climate Change (IPCC) Assessment Report 4 (AR4) likelihood ranges for climate sensitivity ('likely' has a >66% probability, and 'very likely' has a >90% probability; Hegerl *et al* 2007). The vertical black line is CCSM4's climate sensitivity (3.2 °C), the horizontal black line is the maximum global mean, annual mean 20-year trend sampled from the CCSM4 Historical simulations, the black triangle shows the CCSM4 20-year global mean, annual mean trend following SRM cessation (1.16 °C/decade), and the black circle shows the 20-year UD-EBM trend for SRM termination after 65 years of balanced RF (1.0 °C/decade), when the RF jump is roughly equivalent to that estimated in CCSM4 (about 4–5W m⁻²).

trends through SRM is concurrent strong reductions of GHG emissions.

While we have considered here only SRM cessation scenarios within the 21st century, these findings have long-term implications as well. If SRM was used to stabilize global climate under high future GHG emissions, it would need to be maintained on timescales determined by the turnover time of GHGs in the atmosphere, which in the case of carbon dioxide is multiple millennia (Archer 2005). Indeed, the stabilization of global temperature with SRM would also preclude further observations of the climate response to the ongoing GHG emissions (Matthews *et al* 2007), on which many estimates of global climate sensitivity are based. Thus, the large-scale use of SRM to mask business-as-usual GHG emissions could lead to a scenario wherein SRM must be maintained for millennia, else risking a large and uncertain level of rapid global warming upon any unanticipated cessation.

4. Discussion and conclusions

Previous studies have identified the potential for rapid and dangerous global warming following the cessation of SRM (Wigley 2006, Matthews *et al* 2007, Ross and Matthews 2009, Brovkin *et al* 2009, Robock *et al* 2008, McCusker

et al 2012, Irvine *et al* 2012, Jones *et al* 2013). The results presented here reinforce and extend this assessment by (i) quantifying the regional and seasonal climate response to SRM cessation, of critical importance for the impacts on ecological and human systems, and (ii) demonstrating that over a wide range of plausible 21st century scenarios, rates of warming are primarily controlled by the accumulated GHG emissions that are abruptly unmasked upon SRM cessation. Given unabated emissions, the spatial and temporal extent of SAT trends caused by a cessation of SRM would be well beyond the bounds experienced in the last century, and would far exceed those considered safe for many ecological systems (van Vliet and Leemans 2006, Lenton 2011). The spatial structure of the trends precludes the possibility that there will be isolated regions that may experience brief periods of 'relief' from high rates of warming. Moreover, greater than 40% of the land area that experiences warming trends due to SRM cessation also experiences drying trends. Thus, food production could be severely reduced in many regions concurrently under a scenario of high GHG emissions and SRM termination. Furthermore, the adaptive options of many species reach their limits under standard projected climate changes, let alone the widespread and rapid changes that could occur due to SRM cessation. Finally, one potential positive to SRM cessation for photosynthesizing organisms in particular, is increased net primary productivity on land (figures S9 and S10 available at stacks.iop.org/ERL/9/024005/mmedia), however disagreement among global climate models on the sign of the response to cessation (Jones *et al* 2013) leaves this an open question (see supplementary materials for further details available at stacks.iop.org/ERL/9/024005/mmedia).

Alternative climate change mitigation measures could arguably become necessary should climate change progress at a rate or to a degree deemed dangerous to ecological or human systems. Such a scenario could arise if GHG emissions continue unabated, or if climate sensitivity is higher than anticipated. While it has been argued that SRM would be particularly effective in curbing future climate change under high emissions or high climate sensitivity (Ricke *et al* 2012), our results show that the warming following SRM cessation becomes most severe under these same conditions. We are thus left with the disconcerting situation in which SRM is most useful precisely when its associated risks are the greatest. Furthermore, SRM via stratospheric aerosols may introduce a host of additional problems, among them changes in atmospheric and oceanic circulations that act to destabilize the West Antarctic ice sheet (McCusker *et al* 2012) and stratospheric ozone depletion (Tilmes *et al* 2008). It has been suggested that SRM be combined with GHG emissions mitigation with the aim of simultaneously limiting global warming and ocean acidification (Wigley 2006). Our results emphasize that should SRM ever be implemented, aggressive emissions mitigation must occur simultaneously due to the climatic risks involved with its abrupt cessation.

Acknowledgments

The authors wish to thank two anonymous reviewers for helping to substantially improve the manuscript. This research

was funded by the Tamaki Foundation and supported in part by the National Science Foundation through TeraGrid resources provided by the Texas Advanced Computing Center under Grant TG-ATM090059. KCA received support from a James S McDonnell Foundation Postdoctoral Fellowship.

References

- Ammann C M, Washington W M, Meehl G A, Buja L and Teng H 2010 Climate engineering through artificial enhancement of natural forcings: magnitudes and implied consequences *J. Geophys. Res.* **115** D22109
- Archer D 2005 Fate of fossil fuel CO₂ in geologic time *J. Geophys. Res.* **110** C09S05
- Baker M B and Roe G H 2009 The shape of things to come: why is climate change so predictable? *J. Clim.* **22** 4574–89
- Bala G, Duffy P B and Taylor K E 2008 Impact of geoengineering schemes on the global hydrological cycle *Proc. Natl Acad. Sci.* **105** 7664–9
- Battisti D S and Naylor R L 2009 Historical warnings of future food insecurity with unprecedented seasonal heat *Science* **323** 240–4
- Bell G and Collins S 2008 Adaptation, extinction and global change *Evol. Appl.* **1** 3–16
- Bitz C M et al 2012 Climate sensitivity of the community climate system model, version 4 *J. Clim.* **25** 3053–70
- Brovkin V, Petoukhov V, Claussen M, Bauer E, Archer D and Jaeger C 2009 Geoengineering climate by stratospheric sulfur injections: earth system vulnerability to technological failure *Clim. Change* **92** 243–59
- FAO, WFP and IFAD 2012 The State of Food Insecurity in the World 2012. Economic growth is necessary but not sufficient to accelerate reduction of hunger and malnutrition. Rome, FAO www.fao.org/docrep/016/i3027e/i3027e00.pdf
- Gent P R et al 2011 The community climate system model version 4 *J. Clim.* **24** 4973–91
- Hansen J et al 2006 Global temperature change *Proc. Natl Acad. Sci. USA* **103** 14288–93
- Hansen J, Sato M, Kharecha P and von Schuckmann K 2011 Earth's energy imbalance and implications *Atmos. Chem. Phys. Discuss.* **11** 27031–105
- Hegerl G C et al 2007 *Climate Change 2007: The Physical Science Basis. Contribution of Working Group I to the Fourth Assessment Report of the Intergovernmental Panel on Climate Change* ed S Solomon et al (Cambridge: Cambridge University Press) pp 663–745
- Held I M et al 2010 Probing the fast and slow components of global warming by returning abruptly to preindustrial forcing *J. Clim.* **23** 2418–27
- Hoffert M I, Callegari A J and Hsieh C-T 1980 The role of deep sea heat storage in the secular response to climatic forcing *J. Geophys. Res.* **85** 6667–79
- Irvine P J, Sriver R L and Keller K 2012 Tension between reducing sea-level rise and global warming through solar-radiation management *Nature Clim. Change* **2** 97–100
- Jones A et al 2013 The impact of abrupt suspension of solar radiation management (termination effect) in experiment G2 of the Geoengineering Model Intercomparison Project (GeoMIP) *J. Geophys. Res.* **118** 9743–52
- Keith D W, Parson E and Morgan M G 2010 Research on global sun block needed now *Nature* **463** 426–7
- Kravitz B et al 2013 Climate model response from the geoengineering model inter-comparison project (GeoMIP) *J. Geophys. Res.: Atmos.* **118** 8320–32
- Lenton T M 2011 Beyond 2 °C: redefining dangerous climate change for physical systems *Wiley Interdis. Rev.: Clim. Change* **2** 45146
- Lobell D B, Schlenker W and Costa-Roberts J 2011 Climate trends and global crop production since 1980 *Science* **233** 616–20
- Lyman J M et al 2010 Robust warming of the global upper ocean *Nature* **465** 334–7
- Matthews H D and Caldeira K 2007 Transient climate-carbon simulations of planetary geoengineering *Proc. Natl Acad. Sci. USA* **104** 9949–54
- McCusker K E, Battisti D S and Bitz C M 2012 The climate response to stratospheric sulfate injections and implications for addressing climate emergencies *J. Clim.* **25** 3096–116
- Meehl G A et al 2007 *Climate Change 2007: The Physical Science Basis. Contribution of Working Group I to the Fourth Assessment Report of the Intergovernmental Panel on Climate Change* ed S Solomon et al (Cambridge: Cambridge University Press) pp 747–846
- Moss R H et al 2010 The next generation of scenarios for climate change research and assessment *Nature* **463** 747–56
- Rasch P J, Crutzen P J and Coleman D B 2008 Exploring the geoengineering of climate using stratospheric sulfate aerosols: The role of particle size *Geophys. Res. Lett.* **35** L02809
- Rasch P J et al 2008 An overview of geoengineering of climate using stratospheric sulphate aerosols *Philos. Trans. Roy. Soc. A* **366** 4007–37
- Riahi K, Gruebler A and Nakicenovic N 2007 Scenarios of long-term socio-economic and environmental development under climate stabilization *Technol. Forecast. Soc. Change* **74** 887–935
- Ricke K L, Rowlands D J, Ingram W J, Keith D W and Morgan M G 2012 Effectiveness of stratospheric solar-radiation management as a function of climate sensitivity *Nature Clim. Change* **2** 92–6
- Robock A 2000 Volcanic eruptions and climate *Rev. Geophys.* **38** 191–219
- Robock A, Oman L and Stenchikov G L 2008 Regional climate responses to geoengineering with tropical and Arctic SO₂ injections *J. Geophys. Res.* **113** D16101
- Ross A and Matthews H D 2009 Climate engineering and the risk of rapid climate change *Environ. Res. Lett.* **4** 045103
- Schloss C A, Nuñez T A and Lawler J J 2012 Dispersal will limit ability of mammals to track climate change in the Western Hemisphere *Proc. Natl Acad. Sci. USA* **109** 8606–11
- Tilmes S, Müller R and Salawitch R 2008 The sensitivity of polar ozone depletion to proposed geoengineering schemes *Science* **320** 1201–4
- van Vliet A and Leemans R 2006 Rapid species responses to changes in climate require stringent climate protection targets *Avoiding Dangerous Climate Change* ed H J Schellnhuber, W Cramer, N Nakicenovic, T Wigley and G Yohe (Cambridge: Cambridge University Press) pp 135–41
- van Vuuren D P et al 2007 Stabilizing greenhouse gas concentrations at low levels: an assessment of reduction strategies and costs *Clim. Change* **81** 119–59
- Vaughan N E and Lenton T M 2011 A review of climate geoengineering proposals *Clim. Change* **109** 745–90
- Wigley T M L 2006 A combined mitigation/geoengineering approach to climate stabilization *Science* **314** 452–4